Complexation of Copper(II) with Carbonate Ligands in Aqueous Solution: A CW and Pulse EPR Study

P. M. Schosseler,[†] B. Wehrli,[‡] and A. Schweiger*,[†]

Laboratory for Physical Chemistry, Swiss Federal Institute of Technology, 8092 Zürich, Switzerland, and Limnological Research Center, Swiss Federal Institute for Water Resources and Water Pollution Control, 6047 Kastanienbaum, Switzerland

The pH dependent complexation between copper and ^{13}C-labeled carbonate ligands in aqueous solution is investigated by optical spectroscopy and continuous wave and pulse EPR. The small ^{13}C hyperfine coupling observed in the pulse EPR spectra at low temperature and pH 5.5 is assigned to weak, monodentate coordination of carbonates to the Cu^{2+} ion. The ^{13}C hyperfine couplings found at pH 6.5 and 8 are of the same magnitude as twice the nuclear Larmor frequency (matching range) and are assigned to bidentate coordination of carbonate. The larger coupling for the bidentate complexes is explained by a higher covalency of the π bonding in the four-membered ring. The elongation of the axial bonds to the water ligands caused by coordination of carbonate ligands in the equatorial plane of the copper complex leads to smaller proton couplings. The observation of both mono- and bidentate coordination at pH 6.5 and 8 by pulse EPR at low temperature is in contradiction to the calculated concentrations of copper−carbonate complexes at room temperature. Although equilibrium shifts during the freezing of the samples cannot be excluded, the basic mechanisms of mono- and bidentate complexation observed in frozen solution should also apply in aqueous solution at ambient temperature.

I. Introduction

The distribution of trace metals in the aquatic environment is regulated by redox equilibria, the complexation of the metals with organic and inorganic ligands in solution and at surfaces, and precipitation/dissolution reactions.[1] Natural waters in contact with carbonate minerals are characterized by bicarbonate concentrations in the millimolar range. As a consequence the carbonate and bicarbonate ions play a central role in trace metal speciation in many aquatic environments. The precipitation of carbonate minerals in lakes and oceans provides important pathways of trace metal scavenging by adsorption of metal ions or coprecipitation during crystal growth of calcite, siderite, and other carbonate minerals. Knowledge about the interactions between trace metals and carbonate minerals can be used to extract information on chemical changes in aquatic systems by the analysis of sedimentary records.[2] The interaction of metal ions such as Mn^{2+}, Fe^{2+}, Cu^{2+}, and Cd^{2+} with HCO_3^- and CO_3^{2-} ligands and carbonate surfaces has therefore been the subject of numerous thermodynamic and spectroscopic studies.[3−9]

Although these studies have provided deep insight into carbonate chemistry, questions remain regarding the detailed chemical structures of carbonate and bicarbonate complexes. Published complex stoichiometries and stability constants[10] are mainly based on titration and solubility experiments, which often lead to contradictory interpretation of the molecular structures.[3,7] IR and Raman spectroscopies, the methods most commonly adopted for the characterization of carbonate species, allow one to distinguish between mono- and bidentate coordination of carbonate ligands.[11,12] However, a more detailed description of the configuration of the ligands around the metal center in solution is obtained from magnetic resonance spectroscopies.

This study aims at providing more detailed structural information which should allow testing and refining of different models of the copper−carbonate interaction. In order to achieve this goal we make use of UV/vis spectroscopy and continuous wave (CW) and pulse electron paramagnetic resonance (EPR) spectroscopy[13] to investigate the complexation of Cu^{2+} with ^{13}C-labeled carbonate ions in aqueous solution at different pH. The electronic and geometric structures of the complexes obtained from UV/vis and CW EPR investigations can be considerably refined using advanced pulse EPR techniques. Pulse EPR allows one to observe the interactions between the unpaired electron of the Cu^{2+} ion and the magnetic moments of ^{13}C nuclei and protons in the first coordination sphere of the metal ion. The pH dependent substitution of water molecules by carbonate ligands can thus be followed. Copper complexes are well suited for EPR investigations, since the $3d^9$ ion is subject to a Jahn−Teller distortion,[14] so that axial and equatorial coordination sites become easily distinguishable. The hyperfine couplings of the axial and equatorial water protons in the $Cu(H_2O)_6^{2+}$ complex have been determined in a single-crystal CW ENDOR study.[15] The concentrations of mono- and bidentate copper−carbonate

† Swiss Federal Institute of Technology.

‡ Swiss Federal Institute for Water Resources and Water Pollution Control.

⊗ Abstract published in *Advance ACS Abstracts,* September 1, 1997.

(1) Stumm, W.; Morgan, J. J. *Aquatic Chemistry,* 3rd ed.; Wiley Interscience: New York, 1996.

(2) Boyle, E. A. *Geochim. Cosmochim. Acta* **1986,** *50,* 265.

(3) Fouillac, C.; Criaud, A. *Geochem. J.* **1984,** *18,* 297.

(4) Van Cappellen, P.; Charlet, L.; Stumm, W.; Wersin, P. *Geochim. Cosmochim. Acta* **1993,** *57,* 3505.

(5) Morse, J. W. *Mar. Chem.* **1986,** *20,* 91.

(6) McBride, M. B. *Soil Sci. Soc. Am. J.* **1979,** *43,* 693.

(7) Bruno, J.; Wersin, P.; Stumm, W. *Geochim. Cosmochim. Acta* **1992,** *56,* 1149.

(8) Franklin, M. L.; Morse, J. W. *Ocean Sci. Eng.* **1982,** *7,* 147.

(9) Stipp, S. L.; Hochella, M. F., Jr.; Parks, G. A.; Leckie, J. O. *Geochim. Cosmochim. Acta* **1992,** *56,* 1941.

(10) Smith, R. M.; Martell, A. E. *Critical Stability Constants*; Plenum Press: New York, 1976; Vol. 4.

(11) Krishnamurty, K. V.; Harris, G. M.; Sastri, V. S. *Chem. Rev.* **1970,** *70,* 273.

(12) Palmer, D. A.; van Eldik, R. *Chem. Rev.* **1983,** *83,* 651.

(13) Schweiger, A. *Angew. Chem., Int. Ed. Engl.* **1991,** *30,* 265.

(14) Huheey, J. E.; Keiter, E. A.; Keiter, R. L. *Inorganic Chemistry*, 4th ed.; HarperCollins: New York, 1993.

(15) Atherton, N. M.; Horsewill, A. J. *Mol. Phys.* **1979,** *37,* 1349.

Table 1. Concentration of Copper−Carbonate Complexes in Solution at Different pH (Given in % of Total Copper Concentration $Cu_T = 5 \times 10^{-4}$ M) as Calculated with ChemEQL[14] for an Ionic Strength $I = 1$ M at 25 °C

pH	$Cu(H_2O)_6^{2+}$	$Cu(HCO_3)^+$	$Cu(CO_3)^0$	$Cu(CO_3)_2^{2-}$
5.5	60	7	33	∼0
6.5	5	2	83	10
8	∼0	∼0	17	81

complexes in solution at different pH can be estimated from published complexation constants.[3,10]

The results presented in this study also provide the molecular basis for the investigation of the complexation between Cu^{2+} ions and functional groups of the calcite surface.

II. Experimental Section

(A) Speciation Calculations. The speciation of Cu^{2+} with carbonate in solution was calculated using the chemical speciation program ChemEQL.[16] The stability constants of the complexes used in the calculations were taken from the literature.[3,10] The concentrations of $Cu(H_2O)_6^{2+}$, $Cu(HCO_3)^+$, $Cu(CO_3)^0$, and $Cu(CO_3)_2^{2-}$ at 25 °C for a total carbonate concentration of $C_T = 0.05$ M, a total Cu^{2+} concentration of $Cu_T = 5 \times 10^{-4}$ M, and an ionic strength of 1 M at pH 5.5, 6.5, and 8 are given in Table 1. A maximum concentration of $Cu(HCO_3)^+$ is expected at pH 5.5 with $Cu(H_2O)_6^{2+}$ and $Cu(CO_3)^0$ as dominant species, whereas at pH 6.5 $Cu(CO_3)^0$, and at pH 8 $Cu(CO_3)_2^{2-}$, should dominate. Copper hydroxide species that amount only to about 2% at pH 8 are not included in Table 1. The calculations were performed for a closed system with a constant concentration of inorganic carbon.

(B) Sample Preparation. For the preparation of the ^{13}C-labeled carbonate solution, $Ba^{13}CO_3$ (Sigma, 98% enriched) was suspended in water in a closed glass vessel connected through a Teflon tube to a second vessel filled with N_2-saturated distilled water. $Ba^{13}CO_3$ was slowly dissolved by adding concentrated HCl, and $^{13}CO_2$ degassing from the solution was trapped in the second vessel by addition of NaOH. The $^{13}CO_2$ gas not trapped in this procedure was collected in a balloon following the second vessel and bubbled through the aqueous phase until the pH remained constant. The carbonate concentration was determined by titration with KOH and back-titration with $BaCO_3$. Approximately 70% of $^{13}CO_2$ was recovered with this procedure.

An aliquot of 10 mL of the ^{13}C-labeled carbonate solution with a total carbonate concentration of $C_T = 0.06 \pm 0.01$ M was transferred to a closed glass vessel equipped with a pH electrode. NaNO_3 was added to obtain an ionic strength of 1.5 M. The pH of the solution was adjusted to 6.5 with 1 M HNO_3, and 0.5 mL of a 10^{-2} M Cu-$(NO_3)_2$ solution was added, resulting in a total Cu^{2+} concentration of $Cu_T = 5 \times 10^{-4}$ M. After 5 min of stirring, the pH was lowered to 5.5. Degassing of CO_2 resulted in a buildup of pressure in the vessel. With a gas volume of ∼1 mL in the closed vessel, a loss of approximately 13% of carbonate from the solution was estimated at pH 5.5. This loss was smaller than the titration error of the total carbonate concentration and therefore considered to be negligible. Furthermore the degassed CO_2 partially redissolved in the solution at higher pH. A sample was taken after 5 min of stirring, and the pH was raised to 6.5 and 8 with 1 M KOH. After each pH adjustment, the solution was stirred for 5 min and another sample was taken. At pH 8 precipitation of blue-green material was observed after several hours as the solution was highly supersaturated with respect to malachite $(Cu_2CO_3(OH)_2)$. The samples, which did not show any visible precipitation, were immediately transferred to EPR sample tubes and frozen in liquid N_2. The copper−hexaaquo sample was prepared by adjusting the ionic strength of a 5×10^{-4} M $Cu(NO_3)_2$ solution to 1.5 M with NaNO_3.

Two series of samples with and without ^{13}C-labeled CO_2 were prepared under identical conditions to eliminate the strong sodium and nitrogen signals from NaNO_3 that occur in the pulse EPR spectra in the same frequency range as the ^{13}C signals (see below). The addition

of NaNO_3 to the sample solution is required to promote glass formation upon freezing although it makes the pulse EPR measurements more tedious and influences the complexation equilibria (lower K values). Without glass-forming agents such as alcohols or inert salts, crystallization of the solution causes cluster formation of the paramagnetic species in separate phases.[17] Electron−electron dipolar interactions then lead to short relaxation times that make pulse EPR experiments impossible. NaNO_3 was chosen as glass-forming agent since alcohols like ethanol or glycerol act as ligands and were found to severely disturb monodentate carbonate coordination.

(C) Equipment. The UV/vis spectra were measured at room temperature with a Perkin Elmer Lambda 6 spectrophotometer between 200 and 900 nm with a scan speed of 300 nm/min. In addition to the copper−carbonate samples, reference spectra of pure water, 1.5 M NaNO_3 solution, and 0.1 M KHCO_3 solution were recorded to allow for base-line correction of the copper−carbonate spectra and to exclude interference of the copper spectra with the CO_3^{2-} and NO_3^- chromophores. At pH 5.5 base-line distortions were observed due to bubbling of CO_2.

CW EPR spectra were recorded on a Bruker ESP 300 spectrometer equipped with a liquid nitrogen cryostat. Solution spectra at room temperature were measured at a microwave (mw) frequency of 9.776 GHz using a flat cell. Frozen solution spectra were measured at 130 K and 9.483 GHz with a mw power of 5 mW, a modulation amplitude of 0.5 mT, and a modulation frequency of 100 kHz. The magnetic field and the mw frequency were measured with a Bruker NMR gaussmeter ER 035M and a HP 5248M electronic frequency counter, respectively. The accuracy was checked with an *N,N*-diphenylpicryl-hydrazyl (DPPH) reference.

Two-pulse electron spin-echo envelope modulation (ESEEM) experiments and electron nuclear double resonance (ENDOR) experiments were carried out with a home-built X-band pulse EPR spectrometer.[18] The four-pulse ESEEM traces were recorded on a BRUKER ESP 380 spectrometer. All measurements were carried out at 14 K using cooling equipment from Oxford and Cryogenics, at a repetition rate of 1 kHz.

The two-pulse ESEEM time traces were recorded using the pulse sequence $\pi/2-\tau-\pi-\tau-$echo, with pulse lengths of 20 and 40 ns for the $\pi/2$ and π pulses, respectively. The echo intensity was measured as a function of the interpulse delay τ, incremented in steps of 10 ns. The spectrometer dead time was 150 ns. For the ENDOR experiments the stimulated electron spin echo sequence $\pi/2-\tau-\pi/2-T-\pi/2-\tau-$echo was used, with nonselective mw $\pi/2$ pulses and a selective radio frequency (rf) pulse of variable frequency ν_{rf} applied during the time interval T (Mims-ENDOR). The lengths of the mw and rf pulses were 20 ns and 30 μs, respectively, the rf increment was set to $\Delta\nu_{rf} = 50$ kHz, and τ was varied between 200 and 800 ns to avoid signal distortions due to blind spots.

Four-pulse ESEEM experiments were recorded with the pulse sequence $\pi/2-\tau-\pi/2-t_1-\pi-t_2-\pi/2-\tau-$echo, with pulse lengths 24 and 16 ns for the $\pi/2$ and π pulses, respectively. In the 1D combination-peak experiments[19] the echo intensity was measured as a function of time $t_1 = t_2$, incremented from 48 to 4480 ns in steps of 8 ns. To avoid blind spots 30 spectra recorded with τ values from 96 to 576 ns (16 ns steps) were added after data processing. In the 2D HYSCORE experiments[20] the echo intensity was measured as a function of times t_1 and t_2, incremented independently from 48 to 4096 ns in steps of 16 ns. The two-dimensional spectra represent the sum of 16 experiments recorded with τ values from 96 to 352 ns (16 ns steps). Four-step phase cycles were employed in all experiments to eliminate unwanted echo contributions.[19]

(D) Data Manipulation. Data processing was done with BRUKER software (WINEPR) and MATLAB 4.2c (The MathWorks, Inc.). The time traces of the ESEEM data were base-line corrected in one or two dimensions with a fifth-degree polynomial function and apodized with

(16) Müller, B. ChemEQL V2.0, A Program to Calculate Chemical Speciation Equilibria; Internal Report; Limnological Research Center, EAWAG: Kastanienbaum, Switzerland, 1996.

(17) Ross, R. T. *J. Chem. Phys.* **1965**, *42*, 3919.
(18) Wacker, Th. Dissertation ETH Nr. 9913, 1992.
(19) Gemperle, C.; Aebli, G.; Schweiger, A.; Ernst, R. R. *J. Magn. Reson.* **1990**, *88*, 241.
(20) Höfer, P.; Grupp, A.; Nebenführ, H.; Mehring, M. *Chem. Phys. Lett.* **1986**, *132*, 279.

a Hamming window. Zero-filling was performed prior to Fourier transformation. All frequency domain results represent absolute-value spectra.

For two-pulse ESEEM with N nuclei coupled to an unpaired electron the overall echo envelope modulation pattern is given by the product of the N individual modulation patterns[21]

$$E_{mod}(\tau) = \prod_{i=1}^{N} E_i^{mod}(\tau) \tag{1}$$

This property of two-pulse ESEEM was used to eliminate the modulations of the sodium and nitrogen nuclei due to the inert salt $NaNO_3$. The nuclear g_n factors (vide infra) of ^{13}C and ^{23}Na are 1.405 and 1.478, respectively, and both matrix and combination lines of these two nuclei are in the same frequency range. ^{14}N matrix lines ($g_n = 0.404$) occur at lower frequencies and are less disturbing. ESEEM spectra representing only the contributions of ^{13}C nuclei were obtained by dividing the time traces of the ^{12}C (natural isotope ratio) and 98% ^{13}C-labeled carbonate samples. This procedure eliminates the modulations of ^{23}Na, ^{14}N, and ^1H which are identical for the two samples.

In the ENDOR experiments the sodium signal is eliminated by subtracting the ^{12}C from the 98% ^{13}C-labeled carbonate spectra. The intensity of the proton signals was used to scale the spectra. Both procedures are illustrated in the result section.

(E) Theory. The spin Hamiltonian for a spin system with a Cu^{2+} ion (electronic configuration $3d^9$, $S = 1/2$, $I = 3/2$) and ^{13}C nuclei and protons ($I = 1/2$) is given by (in frequency units)

$$\mathcal{H} = \frac{\beta_e}{h}\mathbf{B}_0\mathbf{g}\mathbf{S} + \mathbf{S}\mathbf{A}^{Cu}\mathbf{I} + \mathcal{H}_N \tag{2}$$

where the first term denotes the electron Zeeman interaction with the external magnetic field $\mathbf{B}_0$ and the second term represents the hyperfine interaction between the electron spin S and nuclear spin I of the Cu^{2+} ion. The copper quadrupole interaction is neglected. The $\mathbf{g}$ and $\mathbf{A}^{Cu}$ matrices are assumed to be coaxial and axially symmetric. No distinction is made between the two copper isotopes. The third term $\mathcal{H}_N$ describes the ^{13}C and proton interactions which are small compared to the first and second terms. The CW EPR spectra can therefore be described in first order by the principal values $g_{||}$, $g_\perp$, $A_{||}$, and $A_\perp$ of the $\mathbf{g}$ and $\mathbf{A}^{Cu}$ matrices.

Diagonalization of the first term of the Hamiltonian in eq 2 while neglecting the second term leads to the following nuclear Hamiltonian for each m_S manifold:[22,23]

$$\mathcal{H}_{\alpha,\beta} = \sum_i \left(-\frac{g_n\beta_n}{h}\mathbf{B}_0\mathbf{I}_i + \mathbf{S}'_{\alpha,\beta}\mathbf{A}'\mathbf{I}_i\right) \tag{3}$$

containing isotropic nuclear Zeeman and hyperfine interactions for the ^{13}C nuclei and the protons, denoted by the index i. Diagonalization of this Hamiltonian yields the nuclear frequencies ν_α and ν_β as functions of the magnitudes and relative orientations of the magnetic field and the $\mathbf{g}$ and $\mathbf{A}'_i$ matrices.[24]

For the discussion of our results we neglect the $\mathbf{g}$ anisotropy in the first approximation and assume point dipolar interactions between the electron and nuclear spins. The nuclear frequencies ν_α and ν_β are then given by[25]

$$\left|\begin{matrix}\nu_\alpha \\ \nu_\beta\end{matrix}\right| = \left[\left(\pm\frac{A}{2} + \nu_I\right)^2 + \left(\frac{B}{2}\right)^2\right]^{1/2} \tag{4}$$

with the nuclear Zeeman frequency $\nu_I = -g_n\beta_nB_0/h$. The parameters

A and B are related to the axial hyperfine matrix

$$\mathbf{A} = \begin{bmatrix} A_1 = A_\perp & & \\ & A_2 = A_\perp & \\ & & A_3 = A_{||} \end{bmatrix} = \mathbf{E}a_{iso} + \begin{bmatrix} -T & & \\ & -T & \\ & & 2T \end{bmatrix} \tag{5}$$

by

$$A = A_{||}\cos^2\theta + A_\perp\sin^2\theta = a_{iso} + T(3\cos^2\theta - 1) \tag{6}$$

$$B = (A_{||} - A_\perp)\sin\theta\cos\theta = 3T\sin\theta\cos\theta \tag{7}$$

where θ is the angle between the principal axis of the dipolar coupling matrix ($A_{||}$) and the magnetic field vector $\mathbf{B}_0$.

The dipolar coupling constant T is a function of the nuclear g_n factor and the electron−nuclear distance r:

$$T = \left(\frac{\mu_0}{4\pi}\right)\frac{g_eg_n\beta_e\beta_n}{hr^3} \tag{8}$$

In two-pulse ESEEM spectra of disordered systems with a distribution of θ values it can be of advantage to focus on the combination peaks $\nu_+ = (\nu_\alpha + \nu_\beta)$ or $\nu_- = |\nu_\alpha - \nu_\beta|$ since the basic frequencies ν_α and ν_β may be too broad for detection. In the weak coupling limit ($\nu_I \gg |T + a_{iso}/2|$), the narrow sum combination peak shows a maximum at the frequency position[26]

$$(\nu_\alpha + \nu_\beta)_{max} \cong 2\nu_I + \frac{9}{16}\frac{T^2}{\nu_I} \tag{9}$$

The shift $\Delta_{max} = (9T^2)/(16\nu_I)$ of the sum combination peak maximum from twice the nuclear Zeeman frequency $2\nu_I$ is observed for $\theta \sim 45°$, depending on the magnitude and the anisotropy of the hyperfine coupling. It can be used for an estimation of T, under the assumption that the excitation range of the mw pulses includes the $\theta \sim 45°$ orientations. The concepts described above are schematically illustrated in Figure S1 (Supporting Information) for the weak coupling case.

In two-dimensional HYSCORE spectra of disordered systems the basic frequencies (ν_α, ν_β) are represented by broad correlation ridges in a plot with frequency axes ν_1 and ν_2, the positions and shapes of which are given by the magnitude of the hyperfine interaction.[27] In the weak coupling limit, T and the maximum shift $\Delta\nu_{max}$ of these ridges from the antidiagonal ($\nu_1 = -\nu_2 + \nu_H$), again observed for the $\theta \sim 45°$ orientation, are related by

$$T = \frac{4}{3}\sqrt{\frac{2\nu_I\Delta\nu_{max}}{\sqrt{2}}} \tag{10}$$

Rearrangement of eq 10 and comparison with eq 9 yields the simple relation $\Delta_{max} = \sqrt{2}\Delta\nu_{max}$.

(F) EPR Simulations. The g and A^{Cu} values obtained from the experimental CW EPR spectra at 130 K were refined by simulations performed with the program COMPAR.[28] With COMPAR, strain effects can be considered by using different line widths for the four m_I^{Cu} transitions. For the simulations the $\mathbf{g}$ and $\mathbf{A}^{Cu}$ matrices were assumed to be axially symmetric with coinciding principal axes.

Two-pulse ESEEM spectra were simulated with the program MAGRES.[29] In these simulations electron Zeeman and hyperfine interactions were considered to include the contributions of the four m_I^{Cu} states to the ESEEM spectra. An excitation bandwidth of 50 MHz was assumed for the mw pulses. Time traces were computed and a dead time of 150 ns was introduced prior to the processing of

(21) Mims, W. B. *Phys. Rev. B* **1972**, *5*, 2409.
(22) Rowan, L. G.; Hahn, E. L.; Mims, W. B. *Phys. Rev. A* **1965**, *137*, 61.
(23) Kofman, V.; Shane, J. J.; Dikanov, S. A.; Bowman, M. K.; Libman, J.; Shanzer, A.; Goldfarb, D. *J. Am. Chem. Soc.* **1995**, *117*, 12771.
(24) Hurst, G. C.; Henderson, T. A.; Kreilick, R. W. *J. Am. Chem. Soc.* **1985**, *107*, 7294.
(25) Schweiger, A. In *Modern Pulsed and Continuous Wave Electron Spin Resonance*; Kevan, L., Bowman, M. K., Eds.; Wiley: New York, 1990.

(26) Reijerse, E. J.; Dikhanov, S. A. *J. Chem. Phys.* **1991**, *95*, 836.
(27) Pöppl, K.; Kevan, L. *J. Phys. Chem.* **1996**, *100*, 3387
(28) *COMPAR*, software program ERS300; ZWG-Berlin: Adlershof, 1986.
(29) Keijzers, C. P.; Reijerse, E. J.; Stam, P.; Dumont, M. F.; Gribnau, M. C. M. *J. Chem. Soc., Faraday Trans. 1* **1987**, *83*, 3493.

Table 2. Electronic Transition Energies Estimated from the Optical Spectra

	ν_2 (cm^{-1} ± 100)	ν_3 (cm^{-1} ± 100)
Cu−hexaaquo	12 200	13 500
Cu−carbonate pH 5.5	12 700	14 300
Cu−carbonate pH 6.5/8	13 300	15 400

the data with MATLAB 4.2c. A homogeneous linewidth of 0.3 MHz was used to account for relaxation effects.
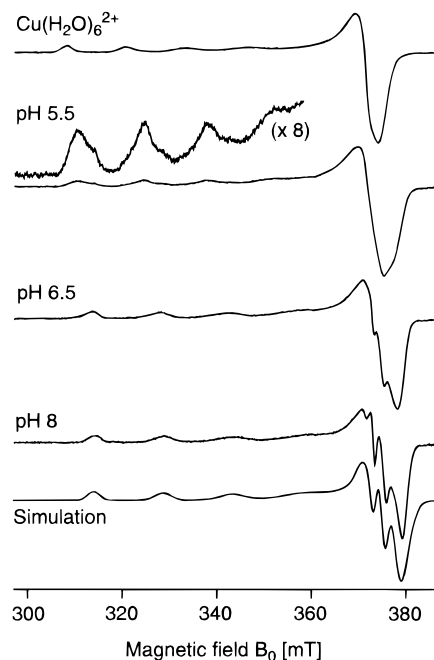
III. Results

(A) Optical Spectra. The UV/vis spectra of the Cu(H$_2$O)$_6^{2+}$ and the copper−carbonate samples at pH 5.5, 6.5, and 8 look very similar and consist of weak, broad bands with λ_{max} values of 810, 780, 760, and 750 nm, respectively. At higher pH the intensity and the width of the bands increase, indicating that a superposition of at least two bands is observed. In agreement with the literature[30] we have assigned these bands to the forbidden d−d transitions d$_{x^2-y^2}$ (B$_{1g}$) ↔ d$_{xy}$ (B$_{2g}$) and d$_{x^2-y^2}$ (B$_{1g}$) ↔ d$_{xz}$, d$_{yz}$ (E$_g$), labeled in the following by ν_2 and ν_3. For the copper−hexaaquo complex the unpaired electron is located in the d$_{x^2-y^2}$ orbital,[13] and we assume the same electronic configuration for the copper−carbonate complexes since the optical and CW EPR spectra (see below) are very similar. The estimated values for ν_2 and ν_3 are given in Table 2.

(B) EPR Spectra. The solution EPR spectrum of Cu-(H$_2$O)$_6^{2+}$ measured at room temperature consists of one broad line centred at $g = 2.19$ (Figure S2, Supporting Information). For the copper−carbonate samples four transitions are resolved and the center of the spectrum is shifted to higher fields with g values of 2.16, 2.16, and 2.15 for pH 5.5, 6.5, and 8, respectively. The splitting of the four lines is approximately 5 mT for all carbonate complexes. The linewidth decreases slightly with increasing pH, leading to a higher resolution.

The frozen solution CW EPR spectra of the same samples measured at 130 K are shown in Figure 1. The principal values of the **g** and **A**^{Cu} matrices obtained from the simulations of these spectra are given in Table 3. These values are typical for axially-distorted octahedral complexes with six oxygen ligands,[31] the parallel direction being defined by the distortion axis. The fits obtained for the pH 8 spectrum with axial **g** and **A**^{Cu} matrices are quite poor as can be seen from the simulation shown in Figure 1. A small orthorhombicity for these matrices can therefore not be excluded. With increasing pH, a decrease of the g values and an increase of the hyperfine couplings is observed, leading to the development of an $A_\perp^{Cu}$ hyperfine pattern in the $g_\perp$ region. At pH 5.5 minor species contribute to the spectrum which can be identified as hexaaquo and pH 6.5 species by comparing the EPR spectra. This is shown in the enlarged inset in Figure 1. Strain effects, arising from the presence of complexes with slightly varying geometries, are observed for all spectra. These geometrical strains lead to a distribution of g and A^{Cu} values which cancel differently in the four m_I^{Cu} states and are responsible for the increasing linewidth at higher fields. The strain effects are more pronounced for the copper−carbonates than for the hexaaquo complex.

(C) ESEEM and ENDOR of ^{13}C. All ^{13}C spectra presented in this section were subjected to the procedure described above to eliminate the sodium, nitrogen, and proton contributions. This procedure is illustrated in Figure S3 (Supporting Information) for the pH 5.5 case.

pH 5.5. Two-pulse ESEEM and Mims ENDOR spectra were recorded at different field positions in the range from $g_\parallel$ to $g_\perp$.

(30) Roos, B. *Acta Chem. Scand.* **1966**, *20*, 1673.
(31) Kivelson, D.; Neiman, R. *J. Chem. Phys.* **1961**, *35*, 149.

Figure 1. CW EPR spectra of the copper−hexaaquo and the copper−carbonate samples in frozen aqueous solution (130 K). The inset for the pH 5.5 spectrum shows an enlarged view of the $g_\parallel$ region to illustrate the presence of several species at this pH. A simulation of the pH 8 spectrum with the parameters given in Table 3 is also shown.

**Table 3.** EPR Parameters of Copper Complexes Measured at 130 K

	$g_\parallel$ (± 0.001)	$g_\perp$ (± 0.001)	$\|A_\parallel^{Cu}\|$ (MHz ± 10)	$\|A_\perp^{Cu}\|$ (MHz ± 10)
Cu−hexaaquo	2.403	2.076	425	25
Cu−carbonate pH 5.5	2.370	2.068	445	35
Cu−carbonate pH 6.5	2.336	2.059	470	40
Cu−carbonate pH 8	2.328	2.056	480	50

Figure 2a shows ESEEM and ENDOR spectra for the observer position $g_\perp$ (314 mT). The same spectra recorded at the $g_\parallel$ observer position (256 mT) are given in Figure S4 (Supporting Information). The prominent features in the ESEEM spectra are the ^{13}C sum combination lines at 5.65 MHz ($g_\parallel$) and 6.9 MHz ($g_\perp$). They are shifted by about 0.2 MHz from twice the nuclear Zeeman frequency $2\nu_C$, calculated from the B_0 field values and indicated by dashed lines in the figures. The basic frequencies ν_α and ν_β, observed as broad features in the range from 1 to 5 MHz, are considerably truncated by the spectrometer deadtime. They are, however, clearly revealed in the ENDOR spectra recorded in the $g_\perp$ region. The spectra show two broad peaks with maxima at 2.5 and 4.5 MHz and linewidths of about 1 MHz, centered around the ^{13}C nuclear Zeeman frequency ν_C = 3.44 MHz. At lower observer fields the signal to noise ratio (S/N) is very poor and the ν_α peak is truncated due to the limited frequency range of the ENDOR amplifier (2−30 MHz). ESEEM and ENDOR spectra recorded at field positions between $g_\parallel$ and $g_\perp$ do not reveal additional information.

pH 6.5/pH 8. The two-pulse ESEEM and Mims ENDOR spectra of the pH 6.5 and 8 samples recorded at different field positions are very similar as illustrated by Figures 2b and 3c. The results obtained from these measurements are therefore treated and discussed together. In Figure 2b ESEEM and ENDOR spectra of the pH 8 sample measured at the $g_\perp$-field position are compared. The prominent features in the ESEEM spectrum are the peaks at 1.5 and 6.8 MHz, the latter one being close to twice the nuclear Zeeman frequency $2\nu_C$ = 6.76 MHz. The ENDOR spectrum shows two peaks at 2.7 and 4.2 MHz of
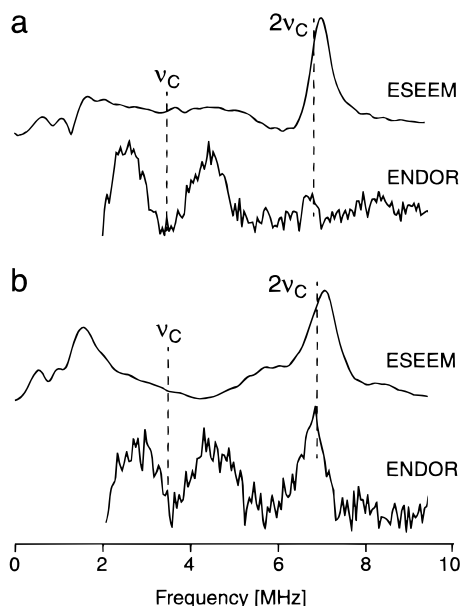
Figure 2. Two-pulse ESEEM and Mims ENDOR spectra of the pH 5.5 sample (a) and the pH 8 sample (b) recorded at the observer field position $g_\perp$. The nuclear Zeeman frequency ν_C of carbon and the sum combination frequency $2\nu_C$ are indicated by dashed lines. The τ values used for the ENDOR measurements are 0.20 μs (a) and 0.23 μs (b). Parameters: mw frequency ν_{mw} = 9.10 GHz (ESEEM), ν_{mw} = 9.27 GHz (ENDOR) (a) and ν_{mw} = 9.12 GHz (ESEEM), ν_{mw} = 9.34 GHz (ENDOR) (b), temperature T = 14 K.

width 1.2 MHz, centered around ν_C = 3.38 MHz, similar to the ENDOR features observed for the pH 5.5 sample (Figure 2a). An additional ENDOR peak at 6.6 MHz is observed at higher pH. If we assign this peak to a ν_β feature, the ν_α peak is expected to occur in the spectral range 0−1 MHz and cannot be observed in the ENDOR spectrum. However, the 6.6 MHz line can be associated with the 1.5 MHz peak found in the ESEEM spectrum. Both the ESEEM and ENDOR spectra thus reveal the presence of at least two different ^{13}C nuclei in the complexes formed at pH 6.5 and 8. Besides a weakly coupled ^{13}C already observed at pH 5.5, a stronger coupled ^{13}C is found with a hyperfine coupling close to $2\nu_C$. Numerical values for $2\nu_C$ range from 5.6 MHz at $g_\parallel$ to 6.9 MHz at $g_\perp$.

Consequently the matching condition is fulfilled,[26,32] where the local magnetic fields set up at the nucleus by the hyperfine and the nuclear Zeeman interaction cancel each other in the ν_α manifold. This leads to a narrowing of the ν_α line and a broadening of the sum combination peak. The effect is illustrated in Figure 3, where two-pulse ESEEM spectra of the pH 6.5 sample, recorded at different B_0-field positions, are shown. The observer fields are indicated by arrows in the echo-detected EPR spectrum in Figure 3 (inset). At field position b (Figure 3b) the intensity of the ν_α peak at 1.6 MHz increases and the sum peak, clearly visible as a narrow feature at 6.8 MHz in Figure 3c, appears as a dip in the broad ν_β peak. The features of the weakly coupled ^{13}C nucleus, hidden by the dominant features of the stronger coupled ^{13}C nucleus in the ESEEM spectra in spectra b and c of Figure 3, can very nicely be observed at the $g_\parallel$-field position (Figure 3a). Here, only spin packets with $\mathbf{B}_0$ approximately along the $g_\parallel$ axis contribute to the spectrum and narrow peaks are observed as a result of this orientation selectivity. The upper bar in Figure 3a indicates the basic frequencies, ν_α and ν_β, and the combination frequencies, ν_+ and ν_-, of the weakly coupled ^{13}C nuclei, the lower bar the corresponding frequencies of the strongly coupled ^{13}C

(32) Lai, H.; Flanagan, H. L.; Singel, D. J. *J. Chem. Phys.* **1988**, *89*, 7161.
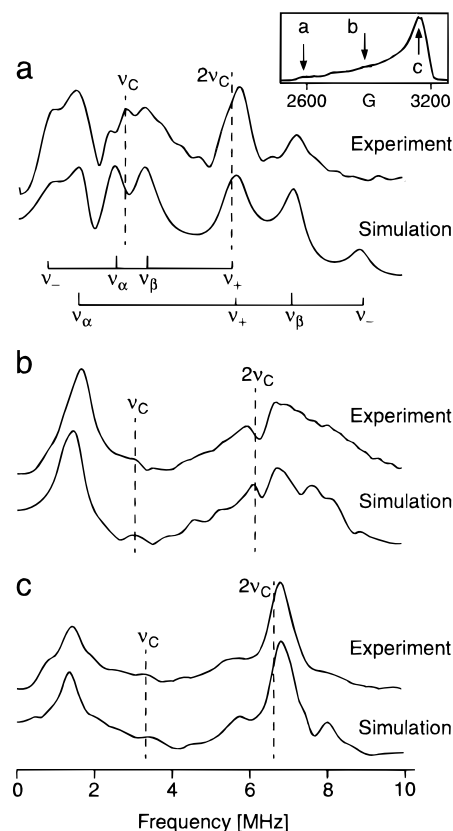
Figure 3. Experimental and simulated two-pulse ESEEM spectra of the pH 6.5 sample, measured at field positions 258 mT (a), 288 mT (b), and 313 mT (c), indicated by arrows in the echo-detected EPR spectrum (inset). The nuclear Zeeman frequency ν_C of carbon and the sum combination frequency $2\nu_C$ are marked by dashed lines for each pair of spectra. The simulation parameters are given in Table 4. The upper bar in part a indicates the basic frequencies, ν_α and ν_β, and the combination frequencies, ν_+ and ν_-, of the weakly coupled ^{13}C nuclei at the $g_\parallel$ position; the lower bar indicates the corresponding frequencies of the strongly coupled ^{13}C nuclei. Mw frequency ν_{mw} = 9.10 GHz, temperature T = 14 K.

Table 4. Hyperfine Matrices of the ^{13}C Carbonate Nuclei for Mono- and Bidentate Coordination, Obtained from the MAGRES Simulations

	coordination	
	monodentate[a]	bidentate[b]
$\lvert A_1^C \rvert$ (MHz)	0.1 ± 0.3	4.0 ± 0.1
$\lvert A_2^C \rvert$ (MHz)	0.1 ± 0.3	6.9 ± 0.1
$\lvert A_3^C \rvert$ (MHz)	3.5 ± 0.3	9.0 ± 0.1

[a] The principal axis A_3^C is tilted by 75° ± 5° with respect to the $g_\parallel$ axis. [b] A_1^C and A_2^C lie in the $g_\perp$ plane; A_3^C is coaxial to the $g_\parallel$ axis.

nuclei. Hyperfine interactions $A^C(g_\parallel)$ of 0.8 and 9 MHz are obtained from the spectrum for the weakly and strongly coupled nucleus, respectively. The latter fulfills the strong coupling condition ($2\nu_I < A^C$); the basic frequencies ν_α and ν_β are therefore centered around $A^C/2$ and split by $2\nu_C$. Simulations carried out with MAGRES (Figure 3) were performed with the parameters given in Table 4 and are discussed below.

(D) One- and Two-Dimensional ESEEM of Protons. Four-pulse sum peak spectra of the copper−hexaaquo complex and the three copper−carbonate samples are compared in Figure 4. The spectra were recorded at 14 K and at the observer field position 310 mT, indicated by an arrow in the echo-detected EPR spectrum of the pH 5.5 sample (inset). At this field position the sum combination peak spectrum of $Cu(H_2O)_6^{2+}$ consists of three lines. The feature close to $2\nu_H$ arises from
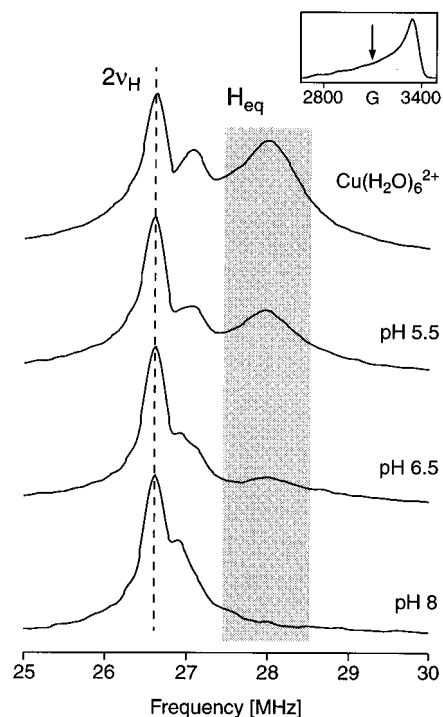
Figure 4. Four-pulse proton ESEEM spectra of the copper−hexaaquo and the copper−carbonate samples at different pH, recorded at the magnetic field position 310 mT, indicated by an arrow in the echo-detected EPR spectrum (inset) of the pH 5.5 sample ($\nu_{mw} = 9.72$ GHz, $T = 14$ K). The spectra represent the sum of 30 signal traces, measured with τ values between 96 and 576 ns (16 ns steps). The dashed line indicates twice the proton Zeeman frequency $2\nu_H$. The shaded area marks the signals which can be unambiguously assigned to protons of equatorial water molecules.

weakly coupled protons of the solvent molecules. The broad line, shifted to higher frequencies by 1.4 MHz, can be unambiguously assigned to protons of water molecules coordinated in the equatorial plane since these protons show the largest hyperfine couplings.[15] The peak shifted by 0.5 MHz arises mainly from the protons of water molecules coordinated in axial positions. This assignment is, however, not unambiguous as there may also be contributions from equatorial protons in this frequency region. In the presence of carbonate ligands, the signal intensity of the equatorial protons decreases with pH (cf. shaded area in Figure 4), assuming that the intensity of the matrix line at $2\nu_H$ is the same for all samples. Simultaneously, position and shape of the proton peak next to the matrix line change. At pH 8 the equatorial proton peak has completely vanished and a new signal shifted by 0.3 MHz from the matrix line is observed.

To distinguish between axial and equatorial contributions to the peak with the 0.5 MHz shift, HYSCORE spectra were recorded for the copper−hexaaquo and copper−carbonate samples at the observer field 310 mT. Two different representations of the copper−hexaaquo spectrum are shown in Figure 5, parts a and b (only one quadrant). Cross peaks of weakly coupled nuclei are observed along the diagonal ($\nu_1 = \nu_2 = 13.2$ MHz), close to the nuclear Zeeman frequency (proton matrix line). Stronger hyperfine couplings shift the cross peaks away from the diagonal. In the HYSCORE spectra in Figure 5a,b the contributions of axial and equatorial protons appear as well-separated ridges to both sides of the matrix peak. The ridges are shifted by 0.35 and 0.85 MHz from the antidiagonal ($\nu_1 = \nu_2 + \nu_H$), respectively. The peak at (15.6, 15.6) MHz is a spectrometer artifact.

The spectrum of the copper−hexaaquo complex can now be compared to the HYSCORE spectra of the pH 5.5 and pH 8
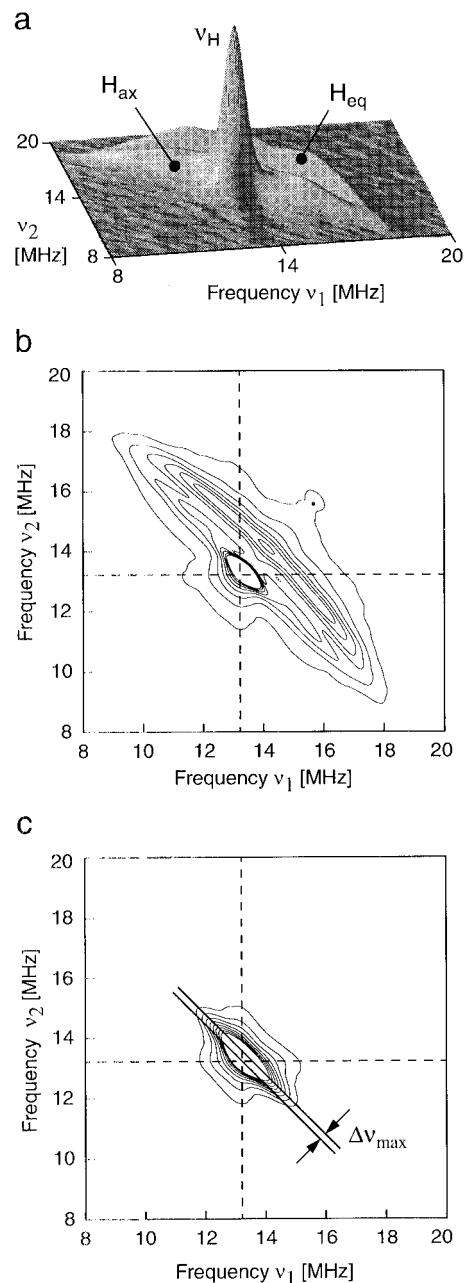
Figure 5. HYSCORE spectra of the copper−hexaaquo complex (a,b) and the pH 8 sample (c). The two-dimensional plots represent the sum of 16 spectra, recorded at the field position 310 mT with τ values between 96 and 352 ns (16 ns steps) ($\nu_{mw} = 9.72$ GHz, $T = 14$ K). (a) Surface plot with the assignment of the spectral features to matrix protons (ν_H) and to protons of axial (H_{ax}) and equatorial (H_{eq}) water molecules. (b) Corresponding contour plot. The dashed lines indicate the proton Zeeman frequency. (c) Contour plot of the pH 8 sample with the same contour levels as in part b. The maximum shift $\Delta\nu_{max}$ of the shoulders from the antidiagonal is indicated by the two solid lines.

samples, shown as contour plots in Figure S5 (Supporting Information) and Figure 5c, respectively. The same contour plot levels were chosen as in Figure 5b, scaled by the matrix line intensity. At pH 5.5 the intensity of both the axial and the equatorial proton ridges has decreased. Close to the matrix peak the shape of the signal is altered, indicating a change in the hyperfine coupling of the axial protons. At pH 8, the matrix line is broadened by two shoulders with a maximum shift of approximately 0.2 MHz from the antidiagonal, as is illustrated in Figure 5c. All ridges from equatorial and axial protons have disappeared.

IV. Discussion

The experimental results presented in the preceding section confirm the formation of different copper—carbonate complexes as a function of pH. In the following we combine the results and propose structures for the complexes in agreement with the coordination chemistry of copper[33] and carbonates.[11,12]

(A) Optical Spectra. The coordination of carbonate to the Cu^{2+} ions leads to an increase of the splitting energies ν_2/ν_3, manifested by a hypsochromic shift in the optical spectra (Table 2). Since carboxylic acids induce weaker ligand fields than water or hydroxyl ions,[14] the increase in energy can be explained by a stronger tetragonal elongation of the Jahn—Teller distorted octahedral copper complexes.[34] Similar electronic spectra with $\lambda_{max} = 675$ nm ($\sim$14 800 cm^{-1}) are observed, for example, for $Cu(oxalate)_2$ complexes.[35] Different coordination schemes are conceivable for chelating ligands like carbonate or oxalate: (1) monodentate complexation at equatorial and axial positions, (2) bidentate complexation in the equatorial plane, and (3) bidentate complexation at an equatorial and an axial position in addition to scheme 2, which defines the equatorial plane. The last possibility is highly improbable as it requires a considerable restriction of the axial elongation. This point is clearly illustrated by the formation constants of copper—ethylenediamine (en) complexes $[Cu(en)_x(H_2O)_{6-2x}]^{2+}$. K_1 and K_2 for $x = 1, 2$ are much higher than K_3 since in the first two cases the coordination takes place in the equatorial plane, whereas the $x = 3$ complexes require coordination of two (en) molecules both at equatorial and axial positions, making a Jahn—Teller distortion difficult.[14] The optical spectra do not, however, allow one to distinguish between mono- and bidentate complexation in the equatorial plane.

(B) EPR Spectra. Further evidence for complex formation is given by the CW EPR spectra recorded at room temperature. Various relaxation mechanisms govern the EPR linewidth of copper complexes in solution like spin rotation and modulation of the g and hyperfine anisotropies through tumbling of the molecules or interconversion of the Jahn—Teller distortion axis.[36,37] For the $Cu(H_2O)_6^{2+}$ ion, fast relaxation leads to one broad resonance without resolved copper hyperfine interaction (Figure S2, Supporting Information). Complexation of carbonate ions hinders the hopping of the distortion axis and decreases the rotational mobility of the complexes. As a result, four hyperfine lines with m_I^{Cu}-dependent widths are observed since the g and hyperfine anisotropies are not equally well averaged out for the four m_I^{Cu} states. The g values obtained at pH 5.5 and 6.5 are very similar; the resolution of the m_I^{Cu} pattern is, however, higher at pH 6.5. The slightly lower g value and the smaller linewidth at pH 8 indicates a further slowdown of the tumbling rate. These findings are in good agreement with the calculated speciation, given in Table 1. The spectra at pH 5.5 and 6.5 can be explained by the formation of the $Cu(CO_3)^0$ complex with considerable contribution of the broad $Cu(H_2O)_6^{2+}$ resonance at pH 5.5. The changes at pH 8 are then due to the coordination of a second carbonate molecule.

At 130 K the molecular motion of the copper complexes is frozen. The g and copper hyperfine parameters given in Table 3 show the similarity of the pH 6.5 and 8 species, confirmed

by the pulse EPR measurements. This result and the occurrence of a further well-defined species at pH 5.5 are in contradiction to the predictions of the speciation calculations. The freezing procedure therefore seems to influence the complexation equilibria; this issue is addressed below. The pH 5.5 spectrum also clearly illustrates the simultaneous occurrence of different complexes at this pH. Smaller variations of the geometry might be reflected by the increasing strain effects at higher pH and the small orthorhombicity of the **g** matrix. The variations of the g and A^{Cu} parameters can be related to an increase of the covalency of the σ and π bonding between the carbonate ions and the Cu^{2+} ion,[31] which is a first hint to the more covalent, bidentate coordination of carbonate ions at higher pH.

(C) ESEEM and ENDOR of ^{13}C. The presence of mono- and bidentate coordination at different pH is clearly revealed by the results of the pulse EPR measurements with ^{13}C-labeled carbonate ligands. At pH 5.5 only a small ^{13}C hyperfine coupling is observed. Using eq 9 and assuming isotropic **g** and axial hyperfine matrices, an isotropic coupling $a_{iso}^C = 1.2$ MHz and a dipolar coupling $T^C = 1.1$ MHz are estimated from the ENDOR spectra and the shift $\Delta_{max} = 0.2$ MHz in the ESEEM spectra (see also Table 4). We assign this coupling to a ^{13}C nucleus of a single carbonate/bicarbonate ion coordinated in the equatorial plane of a monodentate copper—carbonate complex. A tilt of $15° \pm 5°$ of the principal axis of the coupling matrix out of the complex plane is obtained from the simulations of the pH 6.5 sample data. A similar tilt of the monodentate carbonate ligand was found, e.g., in the $[Co(CO_3)_2(H_2O)_4]^{2-}$ complex;[38] it can be explained either by intramolecular hydrogen bonding between carbonate and water molecules in the first coordination sphere or by sterical constraint considerations: the carbonate ligand can only substitute for a smaller water ligand if the planar carbonate π system is twisted out of the equatorial plane. The Cu—C distance of 2.6 Å, obtained from T^C (eq 8), is smaller than the distance of 2.85 Å, estimated from geometrical models ($r_{Cu-O} = 2$ Å, $r_{C-O} = 1.3$ Å, $\angle(Cu-O-C) = 120°$, assuming sp^2 hybridization of the O atom). The small ^{13}C coupling can be compared to the orthorhombic hyperfine coupling of the equatorial water protons of $Cu(H_2O)_6^{2+}$, which show the same connectivity (M—O—H) as the carbonate C atoms.[15] The larger isotropic component observed for the ^{13}C coupling suggests that the delocalization of spin density to the carbonate ligand is higher than to the water ligand and that the ^{13}C hyperfine interaction is expected to be orthorhombic rather than axial. The broad lines observed in our orientationally disordered systems do not allow for a more detailed interpretation.

Bidentate coordination of carbonate ligands to the Cu^{2+} ion takes place at pH 6.5 and 8 and is reflected by the observation of large ^{13}C hyperfine couplings. Such couplings have been observed by Eaton et al.[39] in their investigation of the interaction between ^{13}C-labeled carbonate and copper(II)—transferrin and copper(II)—lactoferrin and have been assigned to direct complexation of the carbonate to the metal ion; however, a detailed analysis is not given in this work. Our parameters for the large hyperfine coupling given in Table 4 are based on simulations of the ESEEM spectra (see Figure 3). For a detailed analysis of the spectra, the orientation selectivity of the mw excitation, the large **g** anisotropy, and contributions of up to four m_I^{Cu} states have to be taken into account. The analysis reveals that the observed spectral features can only be reproduced if the largest principal value of the hyperfine matrix is taken along

(33) Wells, A. F. *Structural Inorganic Chemistry*, 5th ed.; Clarendon Press: Oxford, 1984.

(34) Lever, A. B. P. *Studies in Physical and Theoretical Chemistry 33: Inorganic Electronic Spectroscopy*, 2nd ed.; Elsevier: Amsterdam, 1984.

(35) Eachus, R. S.; Mc Dugle, W. G. *Inorg. Chem.* **1973**, *12*, 1561.

(36) (a) Wilson, R.; Kivelson, D. *J. Chem. Phys.* **1966**, *44*, 154. (b) Wilson, R.; Kivelson, D. *J. Chem. Phys.* **1966**, *44*, 4445.

(37) Atkins, P. W.; Kivelson, D. *J. Chem. Phys.* **1966**, *44*, 169.

(38) Harlow, R. L.; Simonsen, S. H. *Acta Crystallogr.* **1976**, *B32*, 466.

(39) Eaton, S. S.; Dubach, J.; Eaton, G. R.; Thurman, G.; Ambruso, D. R. *J. Biol. Chem.* **1990**, *265*, 7138.

the $g_\parallel$ axis. Further refinement of the spectra is obtained by including in the simulations the contribution of a monodentate carbonate ligand in the equatorial plane. The geometrical arrangement used for these simulations is illustrated in Figure S6 (Supporting Information), together with the orientation of the principal axes systems of the two ^{13}C hyperfine matrices as described in Table 4.

Three different mechanisms may contribute to the covalent bonding of the carbonate ligands to the metal ion; each of them involves different ligand and metal orbitals.[31] If we assume sp^2 hybridization for the oxygen atoms, coordination can take place via (a) σ bonding between the $3d_{x^2-y^2}$ and the sp^2 oxygen orbital. Stabilization of the coordination is obtained through (b) in-plane π bonding between the $3d_{xy}$ and the second sp^2 oxygen orbital, not involved in the C−O bond. Overlap between the $3d_{xz}$ and $3d_{yz}$ metal orbitals and the $2p_z$ oxygen orbital leads to (c) out-of-plane π bonding. Via the $2p_z$ oxygen orbital, electron density from the Cu^{2+} ion can be delocalized through the carbonate π system. The π system of *monodentate* carbonate ligands is tilted with respect to the 3d orbitals of the metal due to intramolecular hydrogen bonding and steric hindrance in the xy plane, making orbital overlap and π bonding more difficult. Polarization of the electron density at the ^{13}C nucleus by the spin density in the carbon $2p_z$ orbital yields explanations for the higher isotropic coupling in the case of *bidentate* complexation and for the orthorhombicity of the large ^{13}C coupling. From the copper−hexaaquo complex it is known that about 5% of the spin density is found on each of the four equatorial water oxygens.[15] A rough model based on point−dipole interactions, with 80% of spin density on the Cu^{2+} ion (at 2.3 Å), 5% spin density on each of the four oxygens (at 1.3 Å), and a spin density of about 0.3% in the $2p_z$ orbital of the C atom (at 0.3 Å, point of maximum electron density[14]) allows one to reproduce the anisotropic part of the large orthorhombic hyperfine matrix with the largest coupling along z. Other mechanisms such as a $Cu(3d_{x^2-y^2})$−C(2s) "transannular overlap" mechanism[40] or a configuration-interaction (CI) mechanism[41] have been proposed to explain the spin density at the ^{13}C nucleus in similar ring systems, leading to large isotropic ^{13}C couplings. Kirmse et al.,[42] for example, have favored the CI mechanism for the explanation of an isotropic ^{13}C coupling of approximately 8 MHz, observed for symmetric Cu/Ni(et$_2$dtc)$_2$ complexes ((et$_2$-dtc)$_2$ = bis(diethyldithiocarbamate)). Without detailed MO calculations it is difficult to attribute the isotropic coupling to the different mechanisms. Spin density delocalization, however, yields a convincing explanation for the anisotropic part of the large ^{13}C coupling.

(D) One- and Two-Dimensional ESEEM of Protons. The ^{13}C couplings reveal monodentate coordination of carbonate at pH 5.5, 6.5, and 8 and an additional bidentate carbonate coordination at pH 6.5 and 8. Since the complexation of carbonate ligands in the first coordination sphere of the Cu^{2+} ions leads to the removal of water molecules, measurement of the proton couplings may yield additional information about the coordination shell. Besides the substitution by carbonates, two other mechanisms can contribute to changes of the proton couplings, (a) deprotonation of coordinated water molecules at higher pH, leading to the formation of copper−hydroxo complexes, and (b) geometrical rearrangements. At a copper concentration of 5×10^{-4} M, hydroxo complexes are not expected to form below pH 6.[43] Above this pH the formation

of binuclear $Cu_2(OH)_2^{2+}$ complexes leads to a decrease of the EPR intensity in the absence of other ligands.

We assign the decrease of the *equatorial* proton signal intensity observed in the four-pulse combination peak and HYSCORE spectra to the substitution of water molecules by carbonate ions. The spectral changes observed for the *axial* protons are mainly due to a change in the coordination. For the equatorial protons an unambiguous assignment is possible at pH 8, where all equatorial coordination positions are occupied by carbonate oxygens, whereas at pH 6.5 contributions of, at maximum, one H_2O/OH^- are still visible. Hydrolysis of the complexes cannot be ruled out in this case. The proton spectra are in agreement with the ^{13}C results since mono- and bidentate coordination of two carbonate ions in the equatorial plane involves at least three coordination positions. At pH 5.5 the strong equatorial proton signal suggests that at the most two water molecules have been replaced by carbonate ions. In the combination peak spectra of $Cu(H_2O)_6^{2+}$ and the pH 8 sample, Δ_{max} shifts of 0.5 and 0.3 MHz were observed for the axial proton couplings, respectively, and corresponding shifts $\Delta\nu_{max}$ of 0.35 and 0.2 MHz were obtained from the HYSCORE spectra. From these results distances of 2.8 and 3.1 Å can be calculated. The first distance is in good agreement with 2.7 Å, obtained from the data of Atherton et al.[15] for the copper−hexaaquo complex ($r_{Cu-O} = 2.2$ Å, $r_{O-H} = 1$ Å, $\angle$(Cu−O−H) = 109°, sp^3 hybridization). From the Cu−H distance of 3.1 Å we then estimate an axial Cu−O distance of about 2.5 Å for the pH 8 sample, which corresponds to an elongation of 0.3 Å of the axial Cu−O bond. The idea of an axial bond elongation due to coordination of carbonate ions in the equatorial plane, suggested by this rough estimation, is supported by the optical spectra. The view is further corroborated by the change in the length of the axial Cu−O bond, observed in compounds like $Na_2Cu(CO_3)_2 \cdot 3H_2O$ ($r_{Cu-O} = 2.36$ Å) or $Cu(OH)_6^{4-}$ ($r_{Cu-O} = 2.81$ Å) with carbonate and hydroxyl ligands in the equatorial plane.[33] Coordination of carbonate ions at axial positions is not considered since it is thermodynamically unfavorable: for copper−amino complexes, for example, the substitution of four water molecules of the $Cu(H_2O)_6^{2+}$ complex by NH_3 ligands is straightforward, whereas the complexation constant K_5 for an axial ligand is 400 times smaller and K_6 has not been reported.[44]

(E) Proposed Structures. In Figure 6 structure proposals for the copper−carbonate complexes, present at pH 5.5, 6.5, and 8 in frozen aqueous solution, are given. As discussed before, mixtures of species are to be expected rather than a single species. This is taken into account by atoms drawn in parentheses in Figure 6, indicating that unambiguous assignments are not possible from the EPR data and that equilibria may allow for the presence of both structures. The arguments supporting our proposals can be summarized as follows:

(a) At pH 5.5 only a small ^{13}C coupling, assigned to monodentate coordination of carbonate in the equatorial plane, and strong hyperfine couplings of two or three equatorial water protons are observed. Internal hydrogen bonding between nonbound carbonate oxygens and coordinated water as well as steric hindrance favor, the trans coordination of carbonates, as is observed for $[Co(CO_3)_2(H_2O)_4]^{2-}$ and $[Co(NH_3)_4CO_3H_2O]$ complexes.[38,45] Species with two carbonates may already show elongation of the Cu−O bond at the axial position. Distinction between species with one or two coordinated carbonates based

(40) White, L. K; Belford, R. L. *J. Am. Chem. Soc.* **1976**, *98*, 4428.
(41) Krishnamoorthy, G.; Prabhananda, B. S. *J. Magn. Reson.* **1978**, *30*, 273.
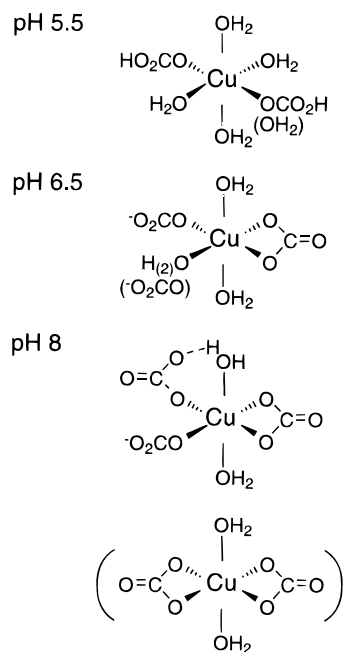(42) Kirmse, R.; Abram, U.; Böttcher, R. *Chem. Phys. Lett.* **1982**, *90*, 9.
(43) Baes, C. F.; Mesmer, R. E. *The Hydrolysis of cations*; Krieger: Malabar, FL, 1986.
(44) Hathaway, B. J.; Tomlinson, A. A. G. *Coord. Chem. Rev.* **1970**, *5*, 1.
(45) Piriz Mac-Coll, C. R. *Coord. Chem. Rev.* **1969**, *4,* 147.

Figure 6. Structure proposals for copper−carbonate complexes in frozen aqueous solution at different pH, as deduced from the experimental results. Features given in parentheses indicate equilibria with possible contributions of both species to the spectra. At pH 8 the presence of complexes with two bidentate rings cannot be excluded.

on the ESE modulation depth[46] is difficult because there is no proper reference system available and the sample contains a mixture of species.

(b) At pH 6.5 the observation of both small and large ^{13}C couplings gives evidence for simultaneous mono- and bidentate complexation of carbonate ions at the central Cu^{2+} ion. The larger covalency of the equatorial bonds leads to an elongation of the axial Cu−O bond. Contributions from strongly coupled protons point to the coordination of one remaining water or hydroxyl ligand in the equatorial plane.

(c) At pH 8 all the equatorial positions are occupied by mono- and bidentate carbonate ligands. Internal H bridging with axial water molecules can stabilize monodentate coordination of carbonate ions. The presence of species with two bidentate carbonate ligands cannot be excluded. Elongated axial Cu−O bonds are observed. The coordination of carbonate at axial positions as well as the formation of four-membered rings between equatorial and axial positions is unlikely, due to the Jahn−Teller stabilization.

For the pH 6.5 and 8 samples, simultaneous mono- and bidentate complexation of carbonate ions at the Cu^{2+} ion is postulated. One could argue that similar spectra are obtained from mixtures of purely monodentate and bidentate species. At pH 8 this would require the presence of approximately equal amounts of bidentate $Cu(CO_3)_2^{2-}$ and monodentate $Cu(CO_3)_4^{6-}$ complexes. The simultaneous formation of these complexes is unlikely, even under nonequilibrium conditions. Furthermore we expect them to show different CW EPR spectra due to the pronounced difference in bonding covalency.

(F) Freezing Effects. The structure proposals deduced from the low-temperature EPR results stress the importance of the monodentate coordination at all pH and suggest higher coordination numbers than the ones expected from commonly accepted complexation constants for copper−carbonate complexes. One could argue that the detailed structures given by

the pulse EPR investigations are more reliable than those calculated from the macroscopic complexation constants. On the other hand the CW EPR spectra recorded at room temperature are in better agreement with the predictions from the speciation calculations. It is therefore important to keep in mind that the pulse EPR measurements are performed in frozen aqueous solutions. The temperature dependence of the ion product of water[1] and of the copper−carbonate complexation may be responsible for considerable equilibrium shifts between room temperature and the freezing point of the solution which is lowered due to the cryoscopic effect of the inert salt. Soli et al.[47] showed, however, that the formation constant of $CuCO_3^0$ decreases at lower temperatures. The same effect has been observed for the formation constants of $CaHCO_3^+$ and $CaCO_3^0$ complexes.[48] The high coordination numbers observed in the frozen aqueous solutions can thus not be explained by the temperature dependence of the complexation constants. Several authors have called attention to the changes in complexation and solution composition that can occur upon freezing.[49,50] Orii et al.[50] have observed local drops in pH of up to 3 units for sodium carbonate−sodium bicarbonate buffers which are due to inhomogeneities of solute concentrations during crystallization (see above). A drop in pH can lead to an acid-catalyzed ring opening,[12] thereby increasing the number of monodentate carbonate ligands. Carbonate concentration gradients in the freezing sample on the other hand could account for the formation of $Cu(HCO_3)_x^{2-x}$ and $Cu(CO_3)_x^{2-2x}$ complexes with $x \geq 2$. In 1 M $KHCO_3$ solutions $Cu(HCO_3)_4^{2-}$ complexes have been reported.[11] These reports suggest that the number of coordinated ligands may have been increased by the freezing procedure.

On the other hand, there is no direct evidence that freezing induces changes in the complexation mechanism of monodentate and bidentate carbonate ligands to the Cu^{2+} ion. Therefore it seems safe to conclude that our complexation model is also valid for the $Cu(HCO_3)^+$ and $Cu(CO_3)^0$ complexes in aqueous solution. From the viewpoint of aquatic chemistry we notice that bidentate coordination of carbonate to the Cu^{2+} ion is the dominant complexation form whereas monodentate coordination should become important only at low pH or at high carbonate concentrations.

V. Conclusions

The combination of different spectroscopic methods and in particular the application of advanced pulse EPR methods has provided detailed information about the geometrical and electronic structures of mono- and bidentate copper−carbonate complexes at different pH. The weakness of the monodentate bonding is reflected by the small interaction observed between the unpaired electron of the Cu^{2+} ion and the ^{13}C nucleus of the carbonate. Although we describe the hyperfine coupling by an axial dipolar interaction matrix, an isotropic coupling $a_{iso}^C > 1$ MHz and the comparison with the hyperfine coupling of equatorial protons suggest that the coupling matrix is orthorhombic rather than axial. Bidentate coordination in the equatorial plane leads to a much larger coupling between the unpaired electron and the ^{13}C carbon, which can be explained by a higher covalency of the bonding and a delocalization of spin density through the π system of the carbonate ion. A detailed analysis of the large hyperfine interaction is made

(46) Kevan, L. In *Modern Pulsed and Continuous Wave Electron Spin Resonance*; Kevan, L., Bowman, M. K., Eds.; Wiley: New York, 1990.

(47) Soli, A. L.; Byrne, R. H. *Limnol. Oceanogr.* **1989**, *34*, 239.
(48) Plummer, L. N.; Busenberg, E. *Geochim. Cosmochim. Acta* **1982**, *46*, 1011.
(49) Basosi, R. *J. Phys. Chem.* **1988**, *92*, 992.
(50) Orii, Y.; Morita, M. *J. Biochem.* **1977**, *81*, 163.

possible by the narrow features observed in the ESEEM spectra that are typical for conditions close to exact cancellation. Complexation in the equatorial plane leads to an increase of the bond length for water ligands coordinated at axial positions. The observation of monodentate carbonate coordination at all pH values that have been investigated is in contradiction to the predictions of speciation calculations based on published equilibrium constants. This result as well as the discrepancies between the CW EPR measurements at room temperature and in frozen solution indicates that pH and concentration changes due to nonideal glass formation might be responsible for equilibrium shifts during freezing. At pH 5.5 and low temperature, only monodentate coordination of bicarbonate to the Cu^{2+} ion is found, whereas at higher pH, both mono- and bidentate carbonate ligands are coordinated in the equatorial plane. The

basic mechanisms of mono- and bidentate complexation observed in the frozen samples should also be valid in aqueous solution at ambient temperature. Bidentate coordination is expected to be the dominant coordination form at ambient temperature.

Supporting Information Available: CW EPR spectra recorded at room temperature, ^{13}C pulse EPR spectra and a HYSCORE spectrum of the pH 5.5 sample, and schematic drawings to illustrate basic EPR concepts and bonding mechanisms (6 pages). Ordering information is given on any current masthead page.

IC9703383